Title

Structure and immunogenicity of the murine astrovirus capsid spike.

Journal

Journal of General Virology, 104(11)

ISSN

0022-1317

Authors

Lanning, Sarah

Pedicino, Natalie

Haley, Danielle J

et al.

Publication Date

2023-11-01

DOI

10.1099/jgv.0.001913

Peer reviewed

JOURNAL OF GENERAL VIROLOGY

RESEARCH ARTICLE

Lanning *et al.*, *Journal of General Virology* 2023;104:001913
DOI 10.1099/jgv.0.001913

MICROBIOLOGY SOCIETY

Structure and immunogenicity of the murine astrovirus capsid spike

Sarah Lanning[1,2], Natalie Pedicino[1], Danielle J. Haley[2], Samuel Hernandez[1], Valerie Cortez[1] and Rebecca M. DuBois[2,*]

Abstract

Human astroviruses (HAstVs) are small, non-enveloped icosahedral RNA viruses that are a significant cause of diarrhoea in young children. Despite their worldwide prevalence, HAstV pathogenesis studies and vaccine development remain challenging due to the lack of an animal model for HAstV infection. The recent development of a murine astrovirus (MuAstV) infection model in mice provides the opportunity to test proof-of-concept vaccines based on MuAstV antigens. To help establish a system in which an astrovirus capsid spike-based vaccine could be tested *in vivo*, we designed and produced a recombinant MuAstV capsid spike protein based on predicted secondary structure homology to HAstV spike proteins. The recombinant MuAstV spike can be expressed with high efficiency in *Escherichia coli* and retains antigenicity to polyclonal antibodies elicited by MuAstV infection. We determined the crystal structure of the MuAstV spike to 1.75 Å and assessed its structural conservation with HAstV capsid spike. Despite low sequence identity between the MuAstV and HAstV spikes and differences in their overall shapes, they share related structural folds. Additionally, we found that vaccination with MuAstV spike induced anti-MuAstV-spike antibodies, highlighting that the recombinant spike is immunogenic. These studies lay a foundation for future *in vivo* MuAstV challenge studies to test whether MuAstV spike can be the basis of an effective vaccine.

INTRODUCTION

Astroviruses are small, nonenveloped, single-stranded, positive-sense RNA viruses named after the 'star-like' appearance of their capsids from when they were first observed in human stool samples by electron microscopy in 1975 [1, 2]. Astroviruses infect a wide range of animal species in both birds and mammals, and mainly spread through the faecal–oral route. In humans, astroviruses are a leading cause of virus-induced diarrhoea in young children, with similar disease severity to that caused by noroviruses [3]. Some studies show astrovirus infections in 2–15% of children hospitalized for diarrhoea [4–6]. Human astroviruses infect most of the human population worldwide, with serology studies revealing that over 90% of adults have anti-HAstV antibodies from a prior infection, and that the presence of these antibodies is associated with a reduction in HAstV disease severity [3, 7–10]. HAstV has eight known classical serotypes (HAstV1–8), with HAstV1 being the most common globally. More recently, divergent strains of HAstV from the VA/HMO and MLB clades have been discovered within the brain and cause fatal encephalitis in immunocompromised humans [11–13]. Despite the prevalence of HAstVs globally, much of their biology and pathogenesis remains unknown, in part due to the lack of an animal model in which to study HAstV infection *in vivo*. In the past, turkey poults and turkey astrovirus (TAstV) were used to study astrovirus pathogenesis [14, 15]. However, turkey husbandry is difficult and turkey models have limited reagents and tools available [16]. Additionally, TAstV is phylogenetically distanced from HAstV, being a part of the avian astrovirus genus, *Avastrovirus*, rather than the mammalian astrovirus genus, *Mamastrovirus*. Protein structural analyses have also revealed strong differences between the TAstV capsid spike domain compared to the HAstV capsid spike domain, suggesting that these two astroviruses may have different interactions with host proteins [17]. Therefore, the need for a more representative animal model system to study astrovirus pathogenesis *in vivo* is necessary.

Received 02 August 2023; Accepted 18 October 2023; Published 01 November 2023
Author affiliations: [1]Department of Molecular Cell and Developmental Biology, University of California Santa Cruz, Santa Cruz, CA, USA; [2]Department of Biomolecular Engineering, University of California Santa Cruz, Santa Cruz, CA, USA.
***Correspondence:** Rebecca M. DuBois, rmdubois@ucsc.edu
Keywords: astroviruses; virus structure; spike protein; murine astrovirus; viral capsid.
Abbreviations: HAstV, human astrovirus; IgG, immunoglobulin G; MuAstV, murine astrovirus; ORF, open reading frame; SEC, size exclusion chromatography; TAstV, turkey astrovirus.
The processed data and model for the MuAstV capsid spike X-ray crystal structure have been deposited with the Protein Data Bank (PDB; https://www.rcsb.org) as entry 8TN8. Data for ELISAs are available upon request from the corresponding author. Murine astrovirus isolate SJ001 accession MK395165.1 (GenBank) derived from persistently infected immunocompromised mice was used for infection studies.

Recent efforts have focused on creating a model system for HAstV in mice using murine astrovirus (MuAstV). MuAstV was first discovered in murine stool samples by electron microscopy during an investigation of a diarrhoea outbreak within a mouse colony in 1985 [18] and has since been found in laboratory mice and wild mice worldwide [19, 20]. MuAstV was not initially considered for an animal model over TAstV due to laboratory mice having a lack of diarrhoea when experimentally infected with MuAstV – unlike turkeys, which experience diarrhoea when infected with TAstV shortly after hatching [21]. However, despite a lack of obvious clinical signs, MuAstV infection in mice presents a promising animal model with which to better understand HAstV infection. MuAstV is phylogenetically more similar to HAstV than TAstV and may consequently have more conserved viral mechanisms with HAstV. Additionally, mice have easier husbandry methods and more genetically engineered models and reagents that can be used to study astrovirus infection *in vivo*. MuAstV infection of live mice can be measured over time by qRT-PCR of stool samples, and some biological similarities have been implicated between MuAstV and HAstV, such as tissue tropism, cellular tropism and host responses to the virus [20, 22–27]. However, whether HAstV and MuAstV have similar virion structures remains unclear.

The HAstV virion consists of a non-enveloped icosahedral capsid, ~40 nm across, sheltering a ~7 kb positive-sense ssRNA genome within the core. The T=3 virion capsid is made up of 180 subunits of the capsid protein, derived from the second genomic open reading frame (ORF2). Intracellular caspase proteolytic processing promotes cellular escape and extracellular proteolytic processing results in maturation into the infectious form [28]. The mature infectious form of HAstV contains an icosahedral shell formed by the capsid core domains with 30 homodimeric capsid spike domains protruding from the 2-fold icosahedral symmetry axes [29]. The HAstV capsid spike domain is thought to be responsible for attachment and entry of the virus [30]. Antibodies targeting the spike domain have been found to neutralize HAstV in cell culture [31–33]. While both the HAstV capsid core and spike domains are immunogenic, only antibodies to the spike domain are able to neutralize HAstV in cell culture, indicating the spike domain as a target for vaccine design [31].

To establish an *in vivo* model in which to study an astrovirus spike-based vaccine, we produced the recombinant MuAstV capsid spike protein, which can be expressed with high efficiency in *Escherichia coli* and retains antigenicity with anti-MuAstV antibodies. Additionally, we solved the high-resolution structure of the MuAstV spike, validating its folding and elucidating structural differences and similarities to the HAstV spike. Finally, we vaccinated mice with recombinant MuAstV spike protein and assessed antibody production, and found that the MuAstV spike induces levels of anti-MuAstV spike IgG antibodies that exceed those generated from natural infection. Our studies establish an *in vivo* system to study an astrovirus spike vaccine.

METHODS

Production of recombinant MuAstV capsid spike protein

The full-length open reading frame of MuAstV capsid protein (ORF2) originating from MuAstV strain SJ001 was retrieved from GenBank #MK395165.1. Known secondary structural features of HAstV1 and HAstV8 spike protein were aligned with secondary structure predictions for the full MuAstV capsid sequence using HHPred [34]. Based on this alignment, the cDNA for MuAstV capsid amino acids 428–676 was codon-optimized for *E. coli* and cloned into a pET52b vector in-frame with an N-terminal methionine and a C-terminal thrombin protease cleavage site and 10× histidine affinity tag (GenScript). This plasmid was transformed into *E. coli* strain T7 express (New England Biolabs) and grown in Luria broth (LB) with 50 µg ml^{-1} ampicillin. Expression of recombinant MuAstV spike was induced with 1 mM isopropyl-β-D-thiogalactopyranoside (IPTG) at 18°C and incubated overnight. *E. coli* cultures were centrifuged at 6000 ***g*** for 15 min, and the *E. coli* pellet was frozen at −20°C overnight. The next day, the *E. coli* pellet was resuspended in Buffer A (20 mM Tris–HCl pH 8, 20 mM imidazole, 500 mM NaCl), containing 1× EDTA-free protease inhibitors (EMD Millipore), benzonase (EMD Millipore #71205-25KUN) and 2.5 mM $MgCl_2$ and was then lysed with ultrasonication. The lysate was centrifuged at 40000 ***g*** for 30 min and the supernatant was 0.22 µm filtered. Packed TALON beads prewashed with Buffer A were incubated with the filtered supernatant on a rotating plane at 4 °C for 1 h. The beads were then placed into a Bio-Spin Chromatography Column (Bio-Rad) and washed 6× with Buffer A. The MuAstV spike was eluted in Buffer B (20 mM Tris–HCl, 500 mM NaCl, 500 mM imidazole, pH 8). Yield was 18 mg of protein from a 1 liter expression. Purified MuAstV spike protein was dialyzed into TBS (10 mM Tris–HCl pH 8, 150 mM NaCl) overnight at 4°C. The cleavable 10× histidine tag was removed from the MuAstV spike protein by incubation with bovine thrombin protease overnight on a rotating plane at 4°C. Cleaved 10× histidine tags were confirmed with SDS-PAGE, with cleavage efficiency near ~100%. The MuAstV spike protein was further purified by size exclusion chromatography (SEC) using a Superdex 75 10/300 GL column in TBS pH 8.

Structural determination of the MuAstV spike

Purified MuAstV spike protein was concentrated to 7 mg ml^{-1} in TBS. MuAstV spike protein crystals were formed in 0.4 µl drops containing a 1:1 ratio of protein solution to well solution containing 0.2 M potassium formate pH 7.3 and 20% (w/v) PEG 3350, using sitting drop vapour diffusion at 22°C. A single crystal was transferred into a cryoprotectant solution consisting of 0.2 M potassium formate pH 7.3, 20% (w/v) PEG 3350 and 25% glycerol, and was then flash frozen into liquid nitrogen. The Advanced Photon Source Beamline 23-ID-D was used to collect a diffraction dataset with wavelength 1.033 Å at cryogenic temperatures. The dataset was processed and scaled using DIALS (ccp4i2) with a resolution cutoff of 1.75 Å. A trimmed model generated by

AlphaFold 2 for the CASP15 competition was used for molecular replacement with Phaser. AutoBuild was used to build an initial model, which was then modelled manually using Coot [35] and refined in Phenix [36] for the final structure.

MuAstV infection and MuAstV spike vaccination studies in mice

Male and female wild-type C57BL/6 weanling mice (3–5 weeks old) were used for the infection studies. Mice were bred within the UCSC vivarium and housed in SPF conditions (n=5 mice/cage). Prior to experiments, animals were confirmed to be negative for MuAstV by qRT-PCR screening of fresh faeces. Briefly, faecal pellets were homogenized and supernatants clarified by centrifugation before RNA was extracted using the QiAmp Viral RNA Mini kit (Qiagen). Copies of the MuAstV genome were quantified using a g-block standard (Integrated DNA Technologies) in a one-step qRT-PCR using TaqMan Fast Advanced Master Mix Virus (Applied Biosystems) with primers (F: TACATCGAGCGGGTGGTCGC, R: GTGTCACTAACGCGCACCTTTTCA) and probe [(6-FAM)-TTTGGCATGTGGGTTAA-(MBGNFQ)] under the following conditions: 50 °C for 5 min and 95 °C for 20 s, followed by 40 cycles of 95°C for 3 s and 60°C for 30 s on a BioRad CFX96 Real Time System. Mice were inoculated orally with 100 µl of 0.22 µm filtered filtrate (100 mg ml^{-1}), corresponding to 3.05×10^6 genome copies of MuAstV strain SJ001, and infection was confirmed by qRT-PCR. At 28 days post-infection, mice were euthanized by cardiac puncture for terminal blood collection. Blood samples were allowed to clot for 30 min at room temperature and then serum was collected by centrifugation at 2000 ***g*** for 15 min at 10°C. For vaccinations, female littermates were immunized intraperitoneally with 50 µg of MuAstV spike protein diluted 1:1 in Complete Freund's Adjuvant (Sigma) for dose 1 followed by three doses in Incomplete Freund's Adjuvant (Sigma). Vaccinations were administered every 2 weeks along with blood collection via submandibular puncture and then terminal bleeds as described above. Prior to vaccination, endotoxin was removed from MuAstV spike using 0.25 ml Pierce High-Capacity Endotoxin Removal Spin Column (Thermo Fisher #88273) using the batch method with a 4°C rotating overnight incubation of the MuAstV spike with the endotoxin removal resin.

Antigenicity studies of MuAstV spike using enzyme-linked immunosorbent assay (ELISA)

Ninety-six-well microtitre ELISA plates (Costar #3590) were coated with 50 µl of 2 µg ml^{-1} purified MuAstV spike in phosphate-buffered saline (PBS), covered with microplate sealing tape (Corning #6575) and incubated overnight at 4 °C. Plates were washed three times (200 µl each) with PBS-T (PBS+0.1% Tween) and dried on a kimwipe. Then 200 µl of blocking solution (PBS-T+5% milk) was added to all wells of the plate and incubated for 1 h at room temperature. The blocking solution was thrown off the plate after incubation and tapped dry on a kimwipe. Then 80 µl of blocking solution was added to all wells. An extra 28 µl of blocking buffer was added to columns 1 and 2. Twelve microlitres of prediluted 1:5 sera from MuAstV-seropositive mice (see previous MuAstV infection methods) or prediluted 1:5 naïve sera was added to the first well in columns 1 and 2, and the remaining sera samples were added to each of the eight rows, making a 1:50 initial dilution on the plate. The multichannel pipette was used to pipette up and down four–six times in column 1 and to transfer 40 µl to column 3. This was repeated until column 11, and the last 40 µl was discarded. The same dilution process was used from column 2 to column 12 to make duplicate dilutions. Plates were incubated with diluted sera at room temperature for 2 h. Plates were then washed three times with 200 µl PBS-T. Goat anti-mouse IgG-HRP secondary antibody (Jackson ImmunoResearch #115-035-071) was diluted 1:3000 in PBS-T+1% milk and 50 µl was added to each well and incubated at room temperature for 1 h. After 1 h incubation, plates were washed three times with 200 µl PBS-T. Immediately before use, two tablets of OPD (Thermo #34006) and 12.5 µl of 30% hydrogen peroxide were added to 25 ml of 0.05 M phosphate citrate buffer (Sigma Aldrich #P4809). 100 µl was added to each well of the plate. Exactly 10 min after the OPD solution was added to the first row, 50 µl of 3M HCl was added to stop the reaction. ELISA plates were read in a plate reader at an absorbance of 490 nm. A control ELISA plate coated with 2 µg ml^{-1} bovine serum albumin (BSA) antigen was run with the same methods.

Immunogenicity studies of MuAstV spike using ELISA

Ninety-six-well microtitre ELISA plates (Costar #3590) were coated with 50 µl of 2 µg ml^{-1} purified MuAstV spike in PBS, covered with microplate sealing tape (Corning #6575) and incubated overnight at 4 °C. Plates were washed three times (200 µl each) with PBS-T and then dried on a kimwipe. Then 200 µl of blocking solution (PBS-T+5% milk) was added to all wells of the plate and incubated for 1 h at room temperature. The blocking solution was thrown off the plate after incubation and tapped dry on a kimwipe. Then 80 µl of blocking solution was added to all wells. An extra 64 µl of blocking buffer was added to row A. Sixteen microlitres of prediluted 1:5 sera from MuAstV spike-vaccinated mice (see previous MuAstV infection methods) was added to the first well in row A, and the remaining sera samples were added to each of the columns, making a 1:50 initial dilution on the plate. The multichannel pipette was used to pipette up and down four–six times in row A and to transfer 80 µl to row B. This was repeated until row H, and the last 80 µl was discarded. Samples were run in duplicate across the columns. Plates were incubated with diluted sera at room temperature for 2 h. They were then washed three times with 200 µl PBS-T. Anti-mouse IgG-HRP secondary antibody (Jackson ImmunoResearch #115-035-071) was diluted 1:3000 in PBS-T+1% milk and 50 µl was added to each well and incubated at room temperature for 1 h. After 1 h incubation, plates were washed three times with 200 µl PBS-T. Immediately before use, two tablets of OPD (Thermo #34006) and 12.5 µl of 30% hydrogen peroxide were added to 25 ml of 0.05 M phosphate citrate buffer (Sigma-Aldrich #P4809). Then 100 µl was added to each well of the plate. Exactly 10 min after OPD solution was added to the first row, 50 µl of 3M HCl was added to stop the reaction. ELISA plates were read in a plate reader at an

absorbance of 490 nm. A control ELISA plate coated with 2 µg ml^{-1} BSA was run with the same methods. ELISAs for naïve sera were run with similar methods, but could not be run in duplicate due to limited sera sample volume, and represent only a single replicate, and for particularly limited sera (mouse 4) the first sample dilution started at 1:100 rather than 1:50.

Phylogenetic analysis of astroviruses with MEGA X

Full astrovirus capsid ORF2 amino acid sequences were aligned using MUSCLE (EMBL-EBI) [37]. The following ORF2 sequences were used: human astrovirus 1, GenBank #AAC34717.1; human astrovirus 2, GenBank #Q82446.1; human astrovirus 3, Uniprot #Q9WFZ0.1; human astrovirus 4, Uniprot #Q3ZN05.1; human astrovirus 5, Uniprot #Q4TWH7.1; human astrovirus 6, Uniprot #Q67815.1; human astrovirus 7, Uniprot #Q96818.2; human astrovirus 8, Uniprot #Q9IFX1.2; human astrovirus MLB1, NCBI #YP_002290968.1; human astrovirus MLB2, GenBank #YP_004934010.1; human astrovirus MLB3, GenBank #YP_006905854.1; human astrovirus VA1, GenBank #YP_003090288.1; human astrovirus VA2, NCBI #ACX83591.2; human astrovirus VA3, NCBI #YP_006905860.1; human astrovirus VA4, NCBI #YP_006905857.1; human astrovirus VA5, GenBank #AJI44022.1; turkey astrovirus 1, GenBank #Q9JH68; turkey astrovirus 2, GenBank #Q9Q3G5; turkey astrovirus 3, GenBank #AY769616.1; mink astrovirus (mamastrovirus 10), GenBank #NC_004579.1; ovine astrovirus (mamastrovirus 13), GenBank #MK211323.1; murine astrovirus SJ002, GenBank #MK395166.1; murine astrovirus SJ001, GenBank #MK395165.1. An evolutionary history of astrovirus species was inferred using the maximum-likelihood method and a Jones–Taylor–Thornton (JTT) matrix-based model [38]. The tree with the highest log likelihood (−27387.34) is shown. The percentage of trees in which the associated taxa clustered together is shown next to the branches. Initial tree(s) for the heuristic search were obtained automatically by applying neighbour-joining and BioNJ algorithms to a matrix of pairwise distances estimated using the JTT model, and then selecting the topology with superior log likelihood value. The tree is drawn to scale, with branch lengths measured in the number of substitutions per site. The tree was rooted using the turkey astroviruses as an outgroup. This analysis involved 23 amino acid sequences. There was a total of 920 positions in the final dataset. Evolutionary analyses were conducted in MEGA X [39].

Pairwise identity analysis between MuAstV spikes and HAstV spikes

Pairwise identity between astrovirus spike sequences was calculated using MUSCLE (EMBL-EBI) alignment. Accession numbers for MuAstV spike and the human astrovirus spikes were the same as those included in the phylogenetic analysis section. The following amino acid residues corresponding to spike domains within the ORF2 capsid protein were used: HAstV1, 431–644; HAstV2,429–644; HAstV3, 432–645; HAstV4, 430–644; HAstV5, 429–641; HAstV6, 430–642; HAstV7, 431–644; HAstV8, 490–705; HAstV-MLB1, 420–646; HAstV-MLB2, 417–643; HAstV-MLB3, 417–643; HAstV-VA1, 408–682; HAstV-VA2, 404–688; HAstV-VA3, 388–691; HAstV-VA4, 408–685; HAstV-VA5, 406–678.

Conservation analysis of MuAstV spike residues

Fifteen MuAstV ORF2 sequences were selected from the CLEAN_UNIPROT database using HMMER to search for unique non-redundant sequences between 15–99% identity to the spike from the SJ001 strain used for the MuAstV spike protein construct. The following MuAstV ORF2 sequences were used: A0A7G9ZE80, A0A2S0SZ07, A0A866W0H6, A0A1Z2YAL6, A0A482N8A3, A0A866W226, K0BXK4, K0BZ51, K0C113, K0C109, A0A6B9KGG5, I3PL98, A0A482N9T7, R4MSW9 and A0A866W2R1. These sequences were aligned with the MuAstV spike sequence (amino acids 428–676, GenBank #MK395165.1) using MUSCLE. Conservation was mapped in ChimeraX with a deep red colour representing the highest conserved residues for this alignment with an ALCO2 value of 0.61 between all 15 sequences and teal representing the maximum variable residues for this alignment with an ALCO2 value of −3.54.

Conservation analysis of HAstV1 spike residues

Eight HAstV sequences corresponding to the eight classical serotypes for HAstV1-8 were aligned using MUSCLE and conservation was mapped onto the HAstV1 spike structure (PDB:5EW0). The following sequences were used for the alignment: human astrovirus 1, GenBank #AAC34717.1; human astrovirus 2, GenBank #Q82446.1; human astrovirus 3, Uniprot #Q9WFZ0.1; human astrovirus 4, Uniprot #Q3ZN05.1; human astrovirus 5. Uniprot #Q4TWH7.1; human astrovirus 6, Uniprot #Q67815.1; human astrovirus 7, Uniprot #Q96818.2; human astrovirus 8, Uniprot #Q9IFX1.2. Conservation was mapped in ChimeraX with a deep red colour representing the maximum conserved residues for this alignment with an ALCO2 value of 1.54 between sequences and teal representing the maximum variable residues for this alignment with an ALCO2 value of −1.87.

RESULTS

Production of recombinant MuAstV capsid spike protein

The MuAstV capsid spike sequence homology to HAstV capsid spike sequences is low (<18% amino acid identity), similar to the low homology between the capsid spikes from the three different HAstV clades (Fig. 1a, b). Reasoning that the spike domains would have structural homology, even in the absence of sequence homology, we used the HHPred server to predict MuAstV capsid secondary structural homology to HAstV1 and HAstV8 spike structures [40]. Based on this predicted secondary structure

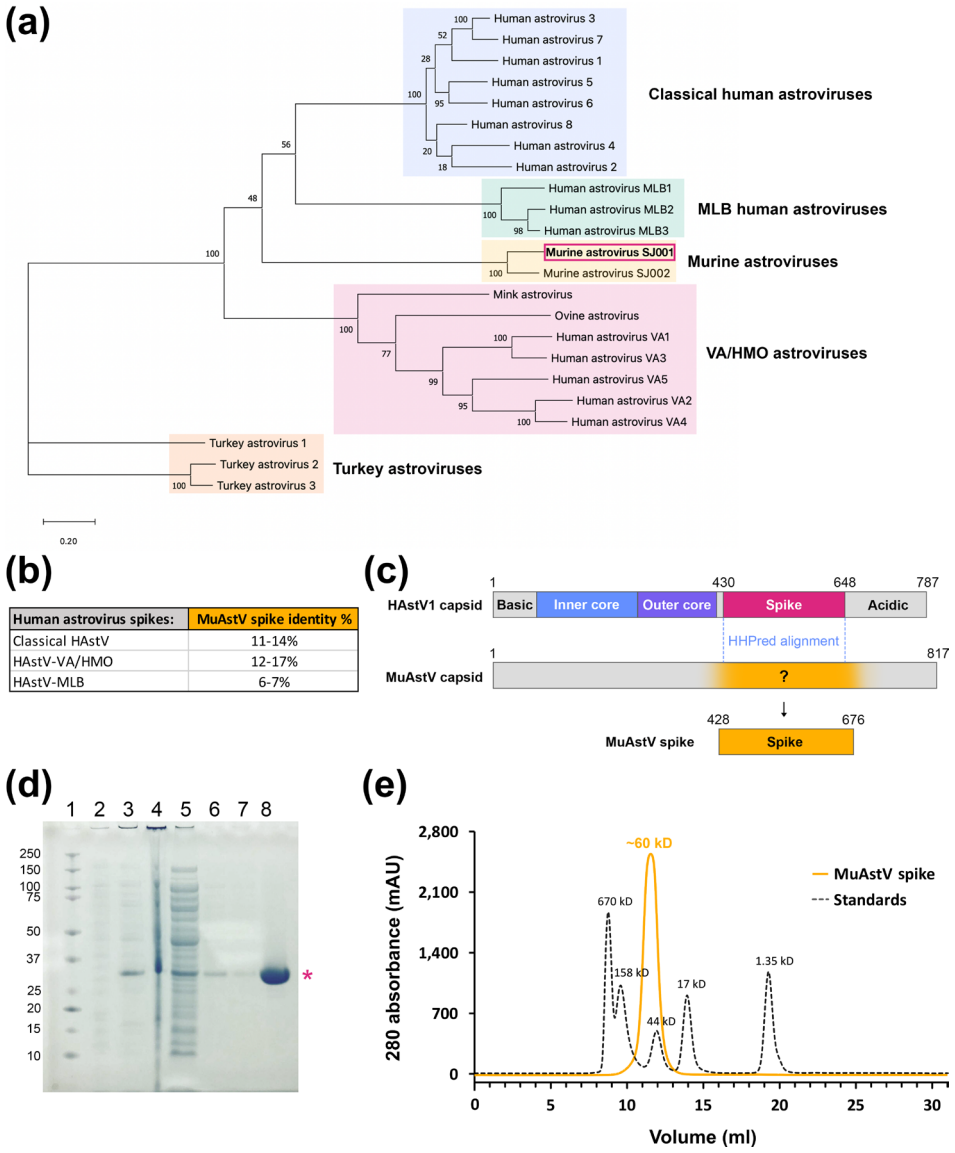

Fig. 1. Elucidation of the MuAstV capsid spike domain boundaries. (a) Phylogenetic analysis of human astroviruses with several animal astroviruses. Analysis was performed using MEGA X with a MUSCLE (EMBL-EBI) alignment of full-length ORF2 capsid protein sequences and the maximum-likelihood method and a JTT matrix-based model. The tree with the highest log likelihood (−27387.34) is shown. The tree was rooted using turkey astrovirus capsid proteins as an outgroup. (b) Pairwise amino acid sequence identities between MuAstV spike and the human astrovirus spikes, generated using MUSCLE (EMBL-EBI) alignment. (c) Schematic of HHPred alignment prediction of the MuAstV spike domain. HAstV1 ORF2 capsid protein representation with known domains is shown above the MuAstV ORF2 capsid protein, with the subsequent residues chosen for the MuAstV spike domain based on an HHPred secondary structure alignment below. (d) SDS-PAGE analysis of *E. coli* expression and TALON purification of the MuAstV spike, which is indicated with an asterisk. Lane 1, BioRad Precision Plus molecular weight markers; lane 2, *E. coli* lysate pre-induction; lane 3, *E. coli* lysate post-induction; lane 4, *E. coli* insoluble pellet after lysis; lane 5, supernatant flow through after TALON bead incubation; lane 6, wash fraction; lane 7, final wash fraction; lane 8, purified MuAstV spike elution fraction. (e) Size-exclusion chromatography trace of MuAstV spike after histidine affinity tag removal and dialysis into TBS. The black dashed line represents gel filtration standards and the orange line represents the MuAstV spike.

alignment, we designed a MuAstV spike expression plasmid to encode residues 428–676 from the capsid protein of MuAstV isolate SJ001 (Fig. 1c). The recombinant MuAstV spike protein expressed in *E. coli* had high expression and high solubility. The MuAstV spike has a calculated mass of 28 kD (+3 kD cleavable histidine affinity tag), which was validated by reducing SDS-PAGE (Fig. 1d). Size-exclusion chromatography revealed that the purified MuAstV spike protein eluted at an apparent molecular weight of 60 kD, indicating that the spike protein formed a dimer in solution, similar to all other known astrovirus spike proteins (Fig. 1e). These data, in conjunction with the X-ray crystallographic studies described below, confirm that the residues chosen for the recombinant MuAstV spike construct represent accurate terminal boundaries of the MuAstV capsid spike domain.

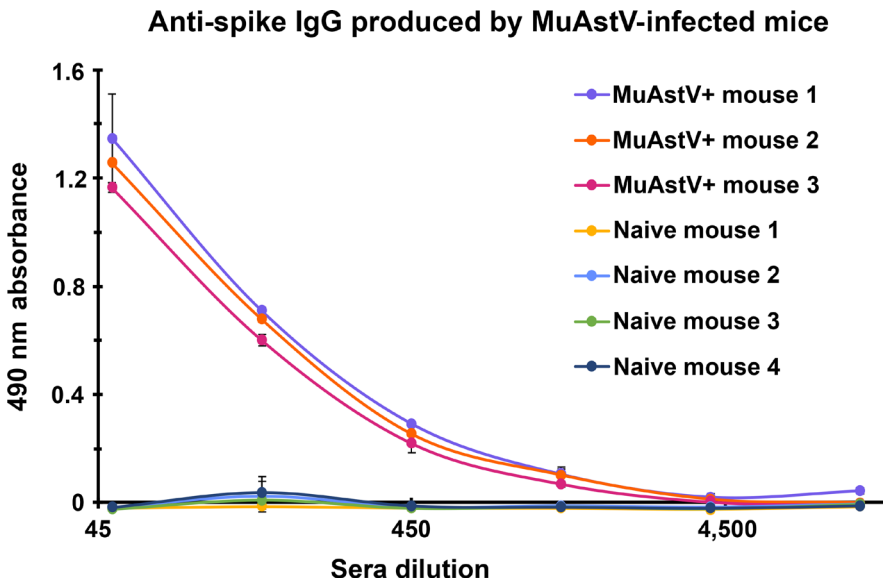

Fig. 2. Recombinant MuAstV spike is antigenic and binds antibodies to native MuAstV. ELISA data showing that serum IgG antibodies from MuAstV-infected mice bind to the recombinant MuAstV spike protein. Naïve mice were not infected with MuAstV. Error bars represent one standard deviation away from mean absorbance of technical duplicates for each serum dilution tested. A matching negative control ELISA plate coated with BSA showed low or no reactivity (<0.11 absorbance at 490 nm), supporting the specificity of the ELISA.

ELISA assessment of recombinant MuAstV spike antigenicity

To validate that the recombinant MuAstV spike retains antigenic epitopes displayed on the native MuAstV virion, we tested whether antibodies in sera from mice infected with MuAstV isolate SJ001 could bind to the recombinant SJ001 MuAstV spike by ELISA. Mice were inoculated with faecal filtrate containing MuAstV, and infection was confirmed with qRT-PCR. Sera were collected 28 days post-infection. The IgG antibodies in polyclonal sera from MuAstV-infected mice showed a strong dose-dependent response to the recombinant MuAstV spike domain by ELISA (Fig. 2a). Naïve mice showed virtually no reactivity (did not exceed 0.0829 absorbance at 490 nm), confirming specificity. These data support that recombinant MuAstV spike displays epitopes found on the native MuAstV virion.

Crystal structure of MuAstV spike and comparison to HAstV spike

To further validate the folding of the recombinant MuAstV spike, we used X-ray crystallography to determine the MuAstV spike structure to 1.75 Å resolution (Fig. 3a, Table 1). Molecular replacement was successful using an AlphaFold2 model generated during the CASP15 competition after deletion of predicted loop residues 441–465 and 564–596. Structural alignment of the experimentally determined MuAstV spike crystal structure with the AlphaFold2 model using TM-align resulted in an RMSD of 2.78 Å across 244 residue pairs and a TM score of 0.84754, revealing a relatively accurate match in the beta-strand regions but significant differences in several surface loops.

The MuAstV spike crystal structure reveals a homodimeric protein (Fig. 3a), consistent with size-exclusion chromatography data, and confirms that the predicted MuAstV spike residues 428–676 form the domain. Interface analysis using the PDBePISA server revealed 1838 Å^2 buried at the dimer interface, with 52–53 interacting residues in each chain (Fig. 3c). Similarly, the dimer interface of the HAstV1 spike is 1835 Å^2, with 50 interacting residues in each chain (Fig. 3d). In addition, both the MuAstV spike and HAstV1 spike structures share an antiparallel beta-barrel fold with a similar folding topology found in all astrovirus spike structures (Fig. 3a, b). Despite these similarities, there are significant differences between MuAstV spike and HAstV1 spike structures. TM-align reveals an RMSD of 4.29 Å across 194 residue pairs and a TM-score of 0.66249. These structural differences result in different overall shapes and surfaces (Fig. 3c, d), most notably with the MuAstV spike containing a large cleft at the top, formed by the two long beta hairpins (β11–β12) from each protomer.

Spherical densities larger than water molecules were observed associated with residues D623, D621 and N641 in both chains A and B (Fig. 4b). A potassium ion was modelled, as it was the best fit for CheckMyMetal parameters [41] in comparison to other ions of similar size or charge (Mg, Na, Ca) that were modelled and tested for coordination chemistry, agreement of experimental B-factors, occupancy and the metal binding environmental motif. Additionally, the crystallography condition in which the MuAstV spike crystallized included potassium formate, which could have been the source of the potassium ion. While this metal-binding site

may be an artefact of crystallization conditions, it is intriguing to note that both aspartates are highly conserved amongst 15 MuAstV strains, suggesting possible functional importance (Fig. 4b).

Conservation analysis of the MuAstV spike

We further sought to identify which regions of the MuAstV spike may be functionally important by mapping conservation across 15 MuAstV sequences onto the MuAstV spike structure. A highly conserved patch of exposed residues (Q474-S476, W511, Q529, R531, R533, W557, D621-D629, Q634, L637, Q675, P676) can be seen on one side of the spike protomer, as indicated by the C site in Fig. 4a. This site includes the potassium ion that was found coordinated with MuAstV spike residues D621, D623 and N641 and water molecules (Fig. 4b). Notably, this site is in a similar location to the relatively conserved S site on the side of the HAstV spike domain (Fig. 4c). Interestingly, within these sites there is short region of amino acids (WVW) that have conserved identity between HAstV and MuAstV. In the HAstV1 spike, this motif faces inward into the beta barrel, which indicates that the high conservation of this sequence is likely involved in the structural stability of the beta barrel core. In the MuAstV spike, the conserved WVW motif is more exposed, with these hydrophobic sidechains facing outward rather than inward, suggesting the possibility that they may be involved in a functional binding interface. Interestingly, the distinctive long beta hairpins (β11–β12) forming the top cleft of the MuAstV spike show higher variability than regions located on the sides of the spike.

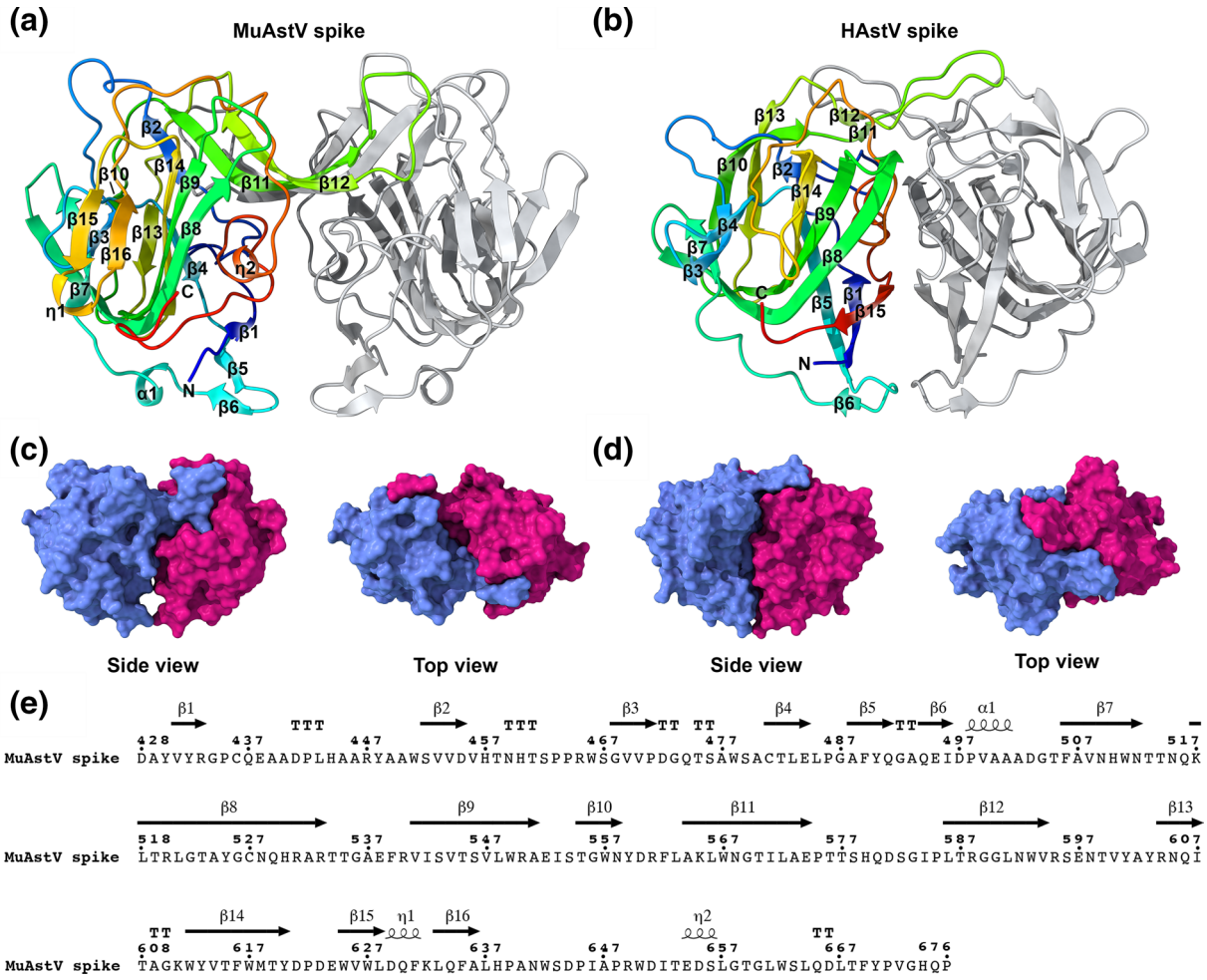

Fig. 3. The MuAstV spike retains a similar folding topology to the HAstV spike but has differences in overall shape. (a) Side view of the MuAstV spike dimer presented as a cartoon model with labelled features on one protomer coloured rainbow from the N-terminus (blue) to the C-terminus (red). (b) Side view of the HAstV1 spike dimer (PDB : 5EW0) presented as a cartoon model. (c) Side and top views of the MuAstV spike dimer presented as a surface model with individual protomers coloured periwinkle and fuchsia. (d) Side and top views of the HAstV1 spike dimer (PDB : 5EW0). (e) Depiction of the secondary structural features of the MuAstV spike, displayed above the amino acid sequences where they occur.

Table 1. Data collection and refinement statistics

	MuAstV spike (PDB code 8TN8)
Data collection:	
Wavelength (Å)	1.0332
Space group	P1
Cell dimensions:	
a, b, c (Å)	45.3285, 48.8724, 65.4627
α, β, γ (°)	93.344, 102.906, 114.696
Resolution (Å)	43.75–1.75 (1.78–1.75)*
R_{merge}	0.048 (0.190)
I/σI	14.4 (1.9)
Completeness	94.79% (92.52%)
Multiplicity	1.7 (1.7)
$CC_{1/2}$	0.995 (0.936)
Refinement:	
Resolution (Å)	43.75–1.75 (1.813–1.75)
No. reflections for refinement	45864
No. reflections for R_{tree}	2293
R_{work}/R_{tree}	0.1706/0.2010
No. atoms	4339
Protein	4015
Ligand/ion	2
Water	322
B-factors (Å^2):	27.11
Protein	26.68
Ligand/ion	31.61
Water	32.41
RMSD:	
Bond lengths(Å)	0.005
Bond angles(°)	0.82
Ramachandran statistics:	
Favoured (%)	97.6
Allowed (%)	2
Outliers (%)	0.4

*Values for the highest resolution shell are shown in parentheses.

Immunogenicity of MuAstV spike

To establish a system in which a spike-based vaccine immunogen could be tested *in vivo*, we assessed whether the recombinant MuAstV spike protein could induce anti-spike IgG antibodies in mice. Female littermates were vaccinated intraperitoneally with three doses of MuAstV spike every 2 weeks and tested for polyclonal anti-MuAstV spike IgG antibodies by ELISA using sera collected pre- and post-vaccination. Post-vaccinated sera showed strong anti-MuAstV spike IgG responses (Fig. 5), indicating that

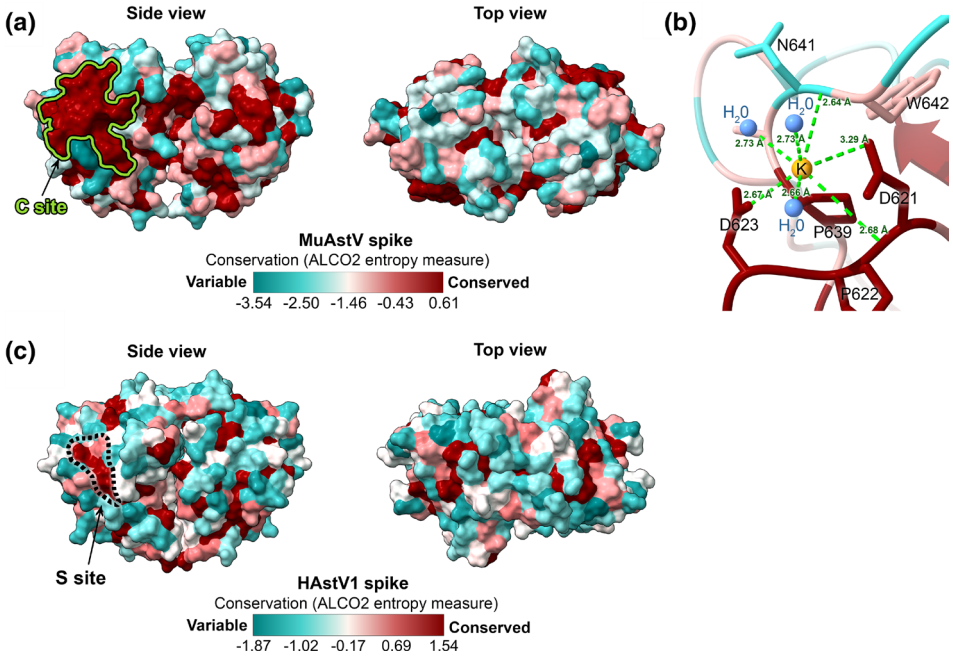

Fig. 4. Conservation analysis of the MuAstV spike reveals a conserved region located on the side of the dimer, and high variability in the upper loop regions. (a) Side and top views of a conservation analysis of the MuAstV spike using 15 MuAstV strain sequences, coloured with highly conserved residues in red, ranging to highly variable residues in teal. A conserved cluster, termed the 'C site', is indicated on the side view. (b) Crystal structure of the MuAstV spike with a potassium ion coordinated to MuAstV spike amino acid residues and water molecules. (c) Side and top views of a conservation analysis of the HAstV1 spike using sequences of the eight known classical serotypes (1–8), coloured with highly conserved residues in red, ranging to highly variable residues in teal. A previously determined conserved cluster termed the 'S-site' is indicated on the side view.

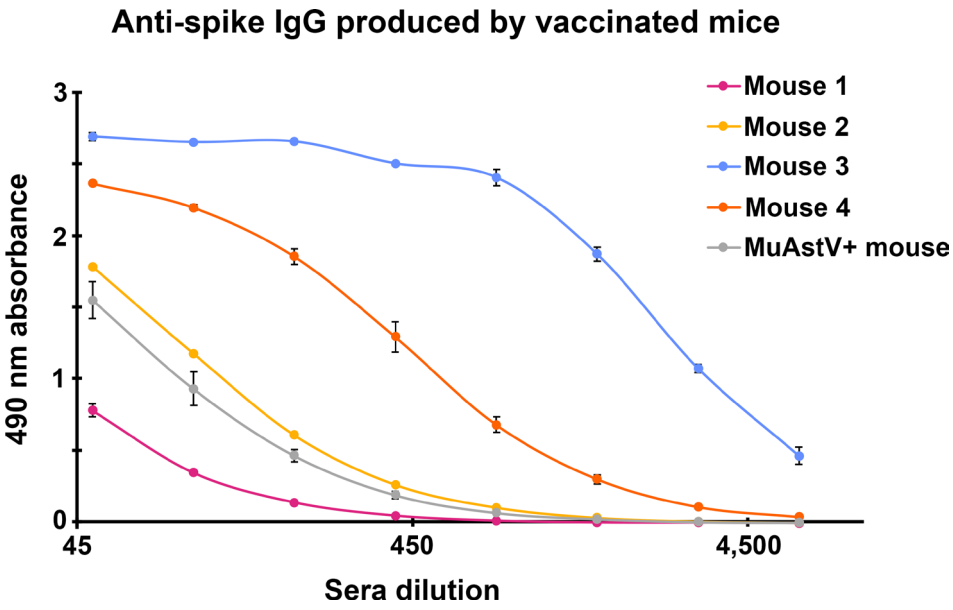

Fig. 5. The MuAstV spike protein is immunogenic and induces anti-MuAstV spike IgG antibodies. ELISA data showing reactivity of IgG antibodies in vaccinated mouse sera to the MuAstV spike from four mice that were vaccinated intraperitoneally with MuAstV spike protein. Sera from a MuAstV seropositive mouse (described previously) were used as a positive control. Error bars represent one standard definition away from mean absorbance of technical duplicates for each sera dilution tested. A matching negative control ELISA plate coated with BSA showed low or no reactivity (<0.08 absorbance at 490 nm), supporting the specificity of the ELISA.

the MuAstV spike protein is immunogenic. Interestingly, three of the four mice had stronger responses than MuAstV-infected mice, although the strength of the responses showed notable variation in individual mice.

DISCUSSION

Here we delineated the boundaries of the recombinant MuAstV capsid spike domain and determined its structure to 1.75 Å resolution, providing information about its evolutionary and functional relationship with HAstV spike. Additionally, we validated that the recombinant MuAstV spike retains antigenicity to antibodies elicited by native MuAstV infection and demonstrated that it can induce robust anti-spike IgG antibodies *in vivo*.

Although the sequence identity between the MuAstV spike and HAstV spike is low, the structural similarities between the two spikes remain more conserved. Similar to the capsid spikes of other astroviruses, the MuAstV spike forms a stable homodimer that is maintained by both hydrophilic and hydrophobic interactions in the dimer interface, as well as by the interactions of the long loops extending from the beta hairpin β11–β12 that overlap onto the top of the opposing protomer (Fig. 3). The dimer interface surface area of the MuAstV spike is remarkably similar to the interface surface area of HAstV1 spike, with a close number of interacting residues, indicating that the structural integrity of the dimer interaction is conserved between the HAstV1 and MuAstV spikes. Furthermore, the MuAstV spike retains an anti-parallel beta barrel at the core of each protomer, as seen in astrovirus spike proteins from other host species, such as HAstV and TAstV. One notable difference between the MuAstV spike structure and that of other astrovirus spikes is the presence of a 'cleft' formed by the two β11–β12 beta hairpins that run along the top of the dimer interface. Additionally, the hole near the base of the spike between the two monomers is more pronounced in the MuAstV spike than in the HAstV spike. Together, these differences result in a different overall shape of the MuAstV spike compared to other astrovirus spikes.

Alignment of the MuAstV spike crystal structure with the same corresponding residues of the AlphaFold 2 model using TM-align revealed a relatively accurate match [42]. The most distinct differences between the structures lay in the same loop residues that needed to be deleted in the AlphaFold 2 model for molecular replacement to succeed. Previous molecular replacement attempts using HAstV1 spike or a SWISS-MODEL-generated model of the MuAstV spike sequence in a HAstV1 spike template found no solution. These trials showed that predictive software such as AlphaFold 2 are better at predicting structure than template-based models in the case of divergent astrovirus spike proteins and therefore may be more useful for generating molecular replacement models for X-ray crystallography.

Based on a sequence alignment of 15 MuAstV strains, a cluster of conserved residues is seen on the side of the MuAstV dimer, which is indicated by the C site in Fig. 4. It is unknown whether these conserved residues indicate a possible host interaction site, or whether this site is necessary for structural integrity. The C site encompasses a similar area on the MuAstV spike monomer face to the previously determined S site on the HAstV spike, a conserved region on the eight classical serotypes of HAstV, but is notably not observed on the divergent MLB spike [40, 43]. Although the C site on the MuAstV spike is in a similar location to the S site on the classical HAstV spikes, most of the sequences differ from those on the S site, aside from the WVW amino acid motif (amino acids 625–627 on MuAstV spike), and there is currently no evidence to suggest that they might interact with the same host factor. Despite this conserved motif, the MuAstV spike has lower similarity in sequence identity to all HAstV spikes (6–17% identity) than the divergent human MLB and VA strain spikes have with the classical HAstV spikes (21–26% identity) [43]. The structure of the human VA spike remains unknown, but it is likely that it does not share sequence similarity with the conserved S-site, given its further divergence from the classical HAstV strains.

The high variability at the top of the MuAstV spike in the β11–β12 hairpin and loop regions is also seen in HAstV spikes, and may indicate a more immunodominant region. In HAstV, this immunodominance is also evidenced by viral escape mutations located in the loop regions in the presence of previously characterized neutralizing monoclonal antibodies [31]. The SJ001 strain of MuAstV has a unique two-amino-acid deletion in relation to similar MuAstV strains between residues 535 and 536 (TTXXGAE) within the extended tip of the loop region of the β8–β9 hairpin, which suggests that this loop may also be under particular selective pressure. Interestingly, all previous structurally characterized neutralizing antibodies that target the HAstV spike have been found to predominantly target loop regions, and have also been shown to prevent the spike from attaching to cells [30], likely by preventing receptor binding. The functional significance of the loops is not known, but given their high variability, their immunodominance could potentially aid the virus by drawing antibodies towards regions of the spike in which the virus can readily mutate without significant consequence to escape neutralization, unlike a functional receptor-binding domain, which faces selective pressure to remain conserved to maintain viral fitness.

A potassium ion was found in the MuAstV spike structure, with associated residues D621, D623 and N641 being highly conserved across MuAstVs. While the N641 residue is not highly conserved, the interaction with the potassium ion is facilitated by the backbone carboxyl oxygen and not the sidechain, so this residue may not need to be conserved in order to maintain an interaction with the potassium. The observation of this potassium ion may be biologically relevant, or it could be a matter of promoting protein crystallization.

The recombinant MuAstV spike produced here represents the first production of the MuAstV spike domain alone to our knowledge, and reflects the native spike domain as assessed by its ability to bind anti-MuAstV antibodies and by its structure. Despite being expressed in a non-native host, the *E. coli*-produced recombinant MuAstV spike retains antigenic epitopes of the native MuAstV spike, similar to what has been seen with HAstV spikes, as well as previously made MuAstV ORF2 capsid constructs such as MuAstV VP70, VP34 and VP27 [44]. A previous study predicted the MuAstV spike, VP25, as amino acids 421–681 of MuAstV ORF2 from the STL1 strain (UniProt K0C109), which is similar but larger than the spike domain boundaries determined here, consisting of amino acids 428–676 from the SJ001 strain (corresponding to amino acids 428–678 in the STL1 strain, due to the two-amino-acid deletion in the β9–β9 hairpin loop in the SJ001 strain) [44]. The determination of the MuAstV spike domain boundaries could allow for easier serological surveillance of MuAstV in vivariums, given the high expression and solubility of the spike domain when expressed, and by providing an alignment template for different MuAstV strains.

We vaccinated mice with recombinant MuAstV spike and show that it is immunogenic and induces anti-spike IgG antibodies. These data, in conjunction with previous mouse vaccinations with recombinant HAstV spike, show that recombinant astrovirus spikes are able to induce anti-spike IgG antibody responses. Although it is currently unknown if the anti-MuAstV spike IgG antibodies are neutralizing (there is not yet an *in vitro* MuAstV infection model to test them), it has previously been shown that antibodies elicited by vaccination with recombinant HAstV spike are capable of neutralizing HAstV in cell culture and can also block HAstV spike attachment to human Caco2 cells [30, 31]. Notably, we show that recombinant MuAstV spike vaccination can induce higher levels of anti-spike IgG antibody than MuAstV infection *in vivo*, as was seen in three of the four mice tested, which presents promising potential to immunize mice against MuAstV using a recombinant spike-based vaccine. Overall, these studies provide a foundation for future proof-of-concept studies to evaluate the ability of MuAstV spike-focused vaccine candidates to protect against MuAstV infection. Future studies may explore different recombinant MuAstV spike doses, adjuvants and routes of vaccination for the ability to protect against infection. Moreover, while we provide strong evidence for the immunogenicity of recombinant MuAstV spike protein, other platforms for spike antigen presentation, including mRNA and viral vectored platforms, such as the recently described rotavirus vaccine-vectored method [45], could be explored.

The MuAstV spike construct we produce here expresses with very high efficiency and could be scaled for mass production, either for use in serology assays or as a vaccine antigen. Our work also provides information about the structural relationships between MuAstV spike and HAstV spike, which could be useful for determining evolutionary relationships, potential cross-species transmission mechanisms, or to further explore the biology of MuAstV infection.

Funding information
This research was supported by the NIH/NIAID grant R01 AI144090 to R.M.D. This research was supported by the NIH/NIAID grant K22 AI156116 to V.C. S. L. and N.P. were supported by the NIH training grant T32 GM133391.

Acknowledgements
This research used the resources of the Advanced Photon Source, a US Department of Energy (DOE) Office of Science user facility operated for the DOE Office of Science by Argonne National Laboratory under contract no. DE-AC02-06CH11357. We thank Sarvind Tripathi for assistance in crystallographic data collection. We thank the University of California, Santa Cruz (UCSC) vivarium staff for their care of the laboratory mice.

Author contributions
R.M.D. and V.C. conceived and designed the project. S.L., N.P. and D.J.H., performed experiments and analysed data. S.H. maintained mouse colonies. S.L. drafted the manuscript and all other authors reviewed and approved the final version.

Conflicts of interest
The authors declare that there are no conflicts of interest.

Ethical statement
All animal experiments were approved by the University of California, Santa Cruz (UCSC) Institutional Animal Care and Use Committee (protocol Cortv2105). UCSC is fully accredited by the Association for the Assessment and Accreditation of Laboratory Animal Care International (AAALAC-I) and has an approved Animal Welfare Assurance Statement on file with the Office of Laboratory Animal Welfare (D16-00493). These guidelines were established by the Institute of Laboratory Animal Resources and were approved by the Governing Board of the US National Research Council.

References

1. Madeley CR, Cosgrove BP. Viruses in infantile gastroenteritis. *Lancet* 1975;2:124.
2. Arias CF, DuBois RM. The astrovirus capsid: a review. *Viruses* 2017;9:15.
3. Olortegui MP, Rouhani S, Yori PP, Salas MS, Trigoso DR, *et al*. Astrovirus infection and diarrhea in 8 countries. *Pediatrics* 2018;141:e20171326.
4. Gaggero A, O'Ryan M, Noel JS, Glass RI, Monroe SS, *et al*. Prevalence of astrovirus infection among Chilean children with acute gastroenteritis. *J Clin Microbiol* 1998;36:3691–3693.
5. Palombo EA, Bishop RF. Annual incidence, serotype distribution, and genetic diversity of human astrovirus isolates from hospitalized children in Melbourne, Australia. *J Clin Microbiol* 1996;34:1750–1753.
6. Shastri S, Doane AM, Gonzales J, Upadhyayula U, Bass DM. Prevalence of astroviruses in a children's hospital. *J Clin Microbiol* 1998;36:2571–2574.
7. Meyer L, Delgado-Cunningham K, Lorig-Roach N, Ford J, DuBois RM. Human astrovirus 1-8 seroprevalence evaluation in a United States adult population. *Viruses* 2021;13:979.
8. Koopmans MPG, Bijen MHL, Monroe SS, Vinjé J. Age-stratified seroprevalence of neutralizing antibodies to astrovirus types

1 to 7 in humans in The Netherlands. *Clin Diagn Lab Immunol* 1998;5:33–37.

9. Kurtz J, Lee T. Astrovirus gastroenteritis age distribution of antibody. *Med Microbiol Immunol* 1978;166:227–230.
10. Kurtz JB, Lee TW, Craig JW, Reed SE. Astrovirus infection in volunteers. *J Med Virol* 1979;3:221–230.
11. Quan PL, Wagner TA, Briese T, Torgerson TR, Hornig M, *et al*. Astrovirus encephalitis in boy with X-linked agammaglobulinemia. *Emerg Infect Dis* 2010;16:918–925.
12. Brown JR, Morfopoulou S, Hubb J, Emmett WA, Ip W, *et al*. Astrovirus VA1/HMO-C: an increasingly recognized neurotropic pathogen in immunocompromised patients. *Clin Infect Dis* 2015;60:881–888.
13. Cordey S, Vu D-L, Schibler M, L'Huillier AG, Brito F, *et al*. Astrovirus MLB2, a new gastroenteric virus associated with meningitis and disseminated infection. *Emerg Infect Dis* 2016;22:846–853.
14. Koci MD, Moser LA, Kelley LA, Larsen D, Brown CC, *et al*. Astrovirus induces diarrhea in the absence of inflammation and cell death. *J Virol* 2003;77:11798–11808.
15. Koci MD, Kelley LA, Larsen D, Schultz-Cherry S. Astrovirus-induced synthesis of nitric oxide contributes to virus control during infection. *J Virol* 2004;78:1564–1574.
16. Cortez V, Meliopoulos VA, Karlsson EA, Hargest V, Johnson C, *et al*. Astrovirus biology and pathogenesis. *Annu Rev Virol* 2017;4:327–348.
17. DuBois RM, Freiden P, Marvin S, Reddivari M, Heath RJ, *et al*. Crystal structure of the avian astrovirus capsid spike. *J Virol* 2013;87:7853–7863.
18. Kjeldsberg E, Hem A. Detection of astroviruses in gut contents of nude and normal mice. Brief report. *Arch Virol* 1985;84:135–140.
19. Ricart Arbona RJ, Kelly S, Wang C, Dhawan RK, Henderson KS, *et al*. Serendipitous discovery of a novel murine astrovirus contaminating a murine helper T-cell line and incapable of infecting highly immunodeficient mice. *comp med* 2020;70:359–369.
20. Yokoyama CC, Loh J, Zhao G, Stappenbeck TS, Wang D, *et al*. Adaptive immunity restricts replication of novel murine astroviruses. *J Virol* 2012;86:12262–12270.
21. Compton SR, Booth CJ, Macy JD. Murine astrovirus infection and transmission in neonatal CD1 mice. *J Am Assoc Lab Anim Sci* 2017;56:402–411.
22. Sebire NJ, Malone M, Shah N, Anderson G, Gaspar HB, *et al*. Pathology of astrovirus associated diarrhoea in a paediatric bone marrow transplant recipient. *J Clin Pathol* 2004;57:1001–1003.
23. Cortez V, Sharp B, Yao J, Livingston B, Vogel P, *et al*. Characterizing a murine model for astrovirus using viral isolates from persistently infected immunocompromised mice. *J Virol* 2019;93:e00223-19.
24. Cortez V, Boyd DF, Crawford JC, Sharp B, Livingston B, *et al*. Astrovirus infects actively secreting goblet cells and alters the gut mucus barrier. *Nat Commun* 2020;11:2097.
25. Ingle H, Hassan E, Gawron J, Mihi B, Li Y, *et al*. Murine astrovirus tropism for goblet cells and enterocytes facilitates an IFN-λ response in vivo and in enteroid cultures. *Mucosal Immunol* 2021;14:751–761.
26. Triana S, Stanifer ML, Metz-Zumaran C, Shahraz M, Mukenhirn M, *et al*. Single-cell transcriptomics reveals immune response of intestinal cell types to viral infection. *Mol Syst Biol* 2021;17:e9833.
27. Kolawole AO, Mirabelli C, Hill DR, Svoboda SA, Janowski AB, *et al*. Astrovirus replication in human intestinal enteroids reveals multicellular tropism and an intricate host innate immune landscape. *PLoS Pathog* 2019;15:e1008057.
28. Banos-Lara M del R, Méndez E. Role of individual caspases induced by astrovirus on the processing of its structural protein and its release from the cell through a non-lytic mechanism. *Virology* 2010;401:322–332.
29. Dryden KA, Tihova M, Nowotny N, Matsui SM, Mendez E, *et al*. Immature and mature human astrovirus: structure, conformational changes, and similarities to hepatitis E virus. *J Mol Biol* 2012;422:650–658.
30. Ricemeyer L, Aguilar-Hernández N, López T, Espinosa R, Lanning S, *et al*. Structures of two human astrovirus capsid/neutralizing antibody complexes reveal distinct epitopes and inhibition of virus attachment to cells. *J Virol* 2022;96:e0141521.
31. Espinosa R, López T, Bogdanoff WA, Espinoza MA, López S, *et al*. Isolation of neutralizing monoclonal antibodies to human astrovirus and characterization of virus variants that escape neutralization. *J Virol* 2019;93:jvi.
32. Bass DM, Upadhyayula U. Characterization of human serotype 1 astrovirus-neutralizing epitopes. *J Virol* 1997;71:8666–8671.
33. Sanchez-Fauquier A, Carrascosa AL, Carrascosa JL, Otero A, Glass RI, *et al*. Characterization of a human astrovirus serotype 2 structural protein (VP26) that contains an epitope involved in virus neutralization. *Virology* 1994;201:312–320.
34. Zimmermann L, Stephens A, Nam S-Z, Rau D, Kübler J, *et al*. A completely reimplemented MPI bioinformatics toolkit with a new HHpred server at its core. *J Mol Biol* 2018;430:2237–2243.
35. Emsley P, Lohkamp B, Scott WG, Cowtan K. Features and development of Coot. *Acta Crystallogr D Biol Crystallogr* 2010;66:486–501.
36. Liebschner D, Afonine PV, Baker ML, Bunkóczi G, Chen VB, *et al*. Macromolecular structure determination using X-rays, neutrons and electrons: recent developments in *Phenix* . *Acta Crystallogr D Struct Biol* 2019;75:861–877.
37. Edgar RC. MUSCLE: multiple sequence alignment with high accuracy and high throughput. *Nucleic Acids Res* 2004;32:1792–1797.
38. Jones DT, Taylor WR, Thornton JM. The rapid generation of mutation data matrices from protein sequences. *Bioinformatics* 1992;8:275–282.
39. Kumar S, Stecher G, Li M, Knyaz C, Tamura K. MEGA X: Molecular Evolutionary Genetics Analysis across computing platforms. *Mol Biol Evol* 2018;35:1547–1549.
40. Dong J, Dong L, Méndez E, Tao Y. Crystal structure of the human astrovirus capsid spike. *Proc Natl Acad Sci U S A* 2011;108:12681–12686.
41. Zheng H, Cooper DR, Porebski PJ, Shabalin IG, Handing KB, *et al*. CheckMyMetal: a macromolecular metal-binding validation tool. *Acta Crystallogr D Struct Biol* 2017;73:223–233.
42. Zhang Y, Skolnick J. TM-align: a protein structure alignment algorithm based on the TM-score. *Nucleic Acids Res* 2005;33:2302–2309.
43. Delgado-Cunningham K, López T, Khatib F, Arias CF, DuBois RM. Structure of the divergent human astrovirus MLB capsid spike. *Structure* 2022;30:1573–1581..
44. Schmidt K, Butt J, Mauter P, Vogel K, Erles-Kemna A, *et al*. Development of a multiplex serological assay reveals a worldwide distribution of murine astrovirus infections in laboratory mice. *PLoS ONE* 2017;12:e0187174.
45. Kawagishi T, Sánchez-Tacuba L, Feng N, Costantini VP, Tan M, *et al*. Mucosal and systemic neutralizing antibodies to norovirus induced in infant mice orally inoculated with recombinant rotaviruses. *Proc Natl Acad Sci U S A* 2023;120:e2214421120.